Petroleum Research 11 (2026) 912–926

Contents lists available at ScienceDirect

Petroleum Research

journal homepage: http://www.keaipublishing.com/en/journals/petroleum-research/

Full Length Article

A new prediction model of bottomhole weight on bit in offshore extended-reach drilling based on the integration of intelligent algorithms and the physical models of rate of penetration

Shuohang Xue [a,b], Yanan Geng [a], Xuyue Chen [b,*], Yi Wu [a], Changsuo Zhou [a], Bingxuan Li [a], Pengbo Li [b]

[a] CNOOC Research Institute Ltd, Beijing, 100028, China
[b] MOE Key Laboratory of Petroleum Engineering, China University of Petroleum, Beijing, 102249, China

ARTICLE INFO

Article history:
Received 27 June 2025
Received in revised form
25 December 2025
Accepted 8 January 2026
Available online 14 January 2026

Keywords:
Bottomhole weight on bit
Intelligent algorithms
Extended-reach well
Offshore drilling
Deepwater drilling
Offshore oil and gas

ABSTRACT

Offshore extended-reach drilling is widely employed for the efficient development of deepwater hydrocarbon fields. However, the complex subsea formation environment and downhole frictional losses lead to significant inaccuracies and limitations in bottomhole weight on bit (WOB) calculations, severely impacting drilling operations. Therefore, this study proposes an improved bottomhole WOB prediction model that combines CNN-BiLSTM networks with Transformer encoders. By introducing a loss function (named DRE) based on the rate of penetration equation into the intelligent algorithm, four models were constructed: CNN-BiLSTM, CNN-Encoder-BiLSTM, CNN-BiLSTM (DRE), and CNN-Encoder-BiLSTM (DRE). The eight models were compared and evaluated, including both the established models and conventional models. Experimental results show that the newly developed CNN-Encoder-BiLSTM (DRE) model parameters' influence degree basically conforms to the DRE with high generalization capability. On the test well, it achieved MAE of 0.859, MRE of 0.1, MAPE of 10%, MSE of 1.201, and R^2 of 0.867, demonstrating good performance. The research results prove that the new model is suitable for bottomhole WOB prediction in offshore extended-reach wells, which is expected to improve drilling efficiency and enable subsequent complex situation analysis, providing new ideas for intelligent drilling research in the marine sector.

© 2026 Chinese Petroleum Society. Publishing services by Elsevier B.V. on behalf of KeAi Communications Co. Ltd. This is an open access article under the CC BY-NC-ND license (http://creativecommons.org/licenses/by-nc-nd/4.0/).

1. Introduction

With the continuous growth of energy demand in all industries around the world, hydrocarbon resources, as an important part of the energy industry, have received increasing attention. Countries around the world have intensified further exploration and development of hydrocarbon resources. At present, numerous studies show that global hydrocarbon exploration and development are gradually expanding to regions such as the ocean and deep water: according to the assessment of the United States Geological Survey (USGS), approximately 47% of the world's undiscovered oil resources and 46% of its undiscovered gas resources are located in marine areas, among them, deepwater and ultra-deepwater oil and gas resources account for 60% of the discovered reserves in the ocean, gradually forming deepwater oil and gas areas including the Gulf of Mexico, West Africa, and the South China Sea (Liu et al., 2020). Furthermore, due to the high oil prices in recent years, the yield rate of offshore oil and gas has generally been above 15%, attracting an increasing number of oil and gas companies to focus on the development of offshore hydrocarbon resources (Yang et al., 2023). In conclusion, it can be seen that the deep-water area of the ocean, as an important region for increasing reserves and production of hydrocarbon resources in the future, holds a significant strategic position. However, in offshore oil drilling operations, extreme seabed conditions (including high-pressure/low-temperature conditions) and complex formation structures (such as fault zones and shallow gas reservoirs) impose more stringent technical requirements and greater challenges on deepwater drilling technologies (Liu et al., 2020; Yang et al., 2023).

* Corresponding author.
E-mail address: chenxuyue2011@163.com (X. Chen).
Peer review under the responsibility of Editorial Office of Petroleum Research.

https://doi.org/10.1016/j.ptlrs.2026.01.005
2096-2495/© 2026 Chinese Petroleum Society. Publishing services by Elsevier B.V. on behalf of KeAi Communications Co. Ltd. This is an open access article under the CC BY-NC-ND license (http://creativecommons.org/licenses/by-nc-nd/4.0/).

At present, in deepwater drilling operations the extended-reach well technology is widely used due to its low cost and the ability to efficiently develop long-distance oil fields (Chen et al., 2014). However, during offshore extended-reach drilling operations, as the drilling depth extends to the highly inclined section, the wellbore friction force acting on the drill string increases, and the frictional loss becomes severe, making it difficult to maintain accurate bottomhole weight on bit (WOB). Bottomhole WOB, as a critical parameter affecting drilling efficiency, may cause accelerated bit wear, drill string buckling or even failure when excessively high, potentially leading to major drilling incidents, polluting the marine environment and even causing casualties; conversely, insufficient bottomhole WOB can result in drilling difficulties and reduced rock-breaking efficiency, causing significant time loss (Abbas et al., 2022; Marck et al., 2014; Zhao et al., 2022). More importantly, as a critical parameter characterizing the interaction between the drill bit and the formation, bottomhole WOB directly reflects the actual downhole dynamics during drilling operations. In contrast, surface WOB data are subject to significant inaccuracies due to complex signal transmission and substantial time delays, making it difficult to reliably distinguish downhole conditions such as drill string sticking and bit balling, which adversely affects the accuracy and timeliness of WOB control. Direct measurement and analysis of bottomhole WOB enable more precise identification of conditions including abnormal bit vibration, bit balling, stuck pipe, and severe bit wear. Such measurement also provides a reliable basis for calculating the actual friction at the bit, thereby supporting timely WOB adjustments and improved drilling efficiency (Marck et al., 2014). This approach compensates for the inability to identify drilling anomalies without downhole sensor data and helps reduce associated costs.

Therefore, accurate prediction of bottomhole WOB is vital for achieving efficient offshore drilling, with significant implications for subsequent offshore drilling complexity analysis, real-time drilling optimization, and feasibility assessment (Chen et al., 2016; Ejike et al., 2024). However, the current bottomhole WOB monitoring technology is still immature, with issues such as low measurement accuracy and poor reliability. The traditional bottomhole WOB calculation methods mainly rely on physical models and empirical formulas, and these methods have limitations in dealing with complex formations and dynamically changing drilling environments. Currently, the maturation of artificial intelligence technology has provided new approaches for efficient drilling. In fact, the integration of artificial intelligence methods with drilling operations has emerged as both a current research focus and future trend in petroleum engineering (Dashevskiy et al., 2008; Salminen et al., 2017). The prediction of bottomhole WOB in offshore drilling by using artificial intelligence technology can improve the ability of drilling operation analysis and real-time monitoring of drilling parameters to a certain extent, minimize the occurrence of incidents, and realize the automation of offshore drilling operations.

The accurate prediction of bottomhole WOB is critically linked to the modeling of the rate of penetration (ROP). However, current research on ROP equations and other physical formulas remains primarily focused on parameter analysis and experimental simulation, which exhibited significant limitations. For instance, Reza and Alcocer (1986) used field data to fit unknown constants and exponents in the Bingham equation through linear regression and validated the sensitivity of the new model via partial derivative analysis. However, their model did not account for the effects of bit type selection and formation environment. Alum and Egbon (2011) analyzed the properties of drilling fluids and summarized the influence of their mechanical performance on the ROP equation, proposing a semi-analytical model that incorporates plastic viscosity. However, this model was developed specifically for certain formation types and drilling fluid systems, and its applicability to other types of drilling fluids was not examined. Shaabani et al. (2016) investigated ROP variations in carbonate rocks through laboratory experiments, revealing a relationship between the weight on bit exponent and the drilling rate exponent, which provides valuable insights for ROP equation modification. However, their experiments did not extend to other lithological conditions. Bilim and Karakaya (2021) established an ROP prediction equation based on rock physical properties and WOB through rock drill ability experiments, yet the model lacked field validation and overlooked other key factors besides WOB in drilling parameters. Atashnezhad et al. (2020) introduced the interfacial friction angle of Polycrystalline Diamond Compact (PDC) bits and developed a corresponding ROP prediction model using a differential evolution algorithm. Nevertheless, the model was solely based on experimental data, had not been extended to other types of drill bits, and lacked validation in actual field applications. Overall, traditional physical methods generally suffer from incomplete factor consideration and limitations in experimental conditions, resulting in insufficient applicability in practical operations.

In contrast, artificial intelligence methods have recently garnered substantial attention and have shown remarkable progress within the drilling domain (Abahusayn et al., 2012; Li et al., 2023). Hegde et al. (2015) developed multiple machine learning models, including a Random Forest (RF) model, for predicting the ROP. The Random Forest model demonstrated the highest prediction accuracy, achieving a Root Mean Square Error (RMSE) of 0.074, however, the study also highlighted that there is a risk of overfitting in this model. Boukredera et al. (2023) developed an artificial neural network-based model for predicting ROP, which achieved an RMSE of 0.017, they also utilized the Particle Swarm Optimization (PSO) algorithm to optimize surface drilling parameters, theoretically reducing drilling time. However, the system could not integrate real-time logging data, limiting its practical applicability in the field. Yehia et al. (2024) compared the accuracy of various machine learning models, including XGBoost, in predicting the ROP, the XGBoost model achieved a coefficient of determination (R^2) as high as 0.91. However, the study was limited to basic model analysis and suffered from insufficient data volume and a lack of field validation. Quitian-Ardila et al. (2024) applied machine learning methods to predict and optimize the rheological behavior of drilling fluids. However, the influence of formation conditions on the results was not sufficiently considered. Urdaneta et al. (2024) employed a Transformer model for predicting the ROP, achieving a Mean Absolute Percentage Error (MAPE) of 5.22%. However, the study also faced the issue of insufficient training data. Alsaihati et al. (2025) integrated multiple machine learning models and optimization algorithms to enhance the ROP and mitigate downhole vibrations, their study ultimately selected the RF model and differential evolution algorithm for drilling parameter optimization, achieving an R^2 value of 0.86. However, the proposed methodology did not adequately account for the conditions of offshore drilling environments, nor did it evaluate the impact of varying formation properties on model performance, which limits its practical applicability.

In addition, some scholars have focused on predicting bottomhole WOB and bottomhole torque. Oyedere and Gray (2020) expanded drilling data using a Generative Adversarial Network and subsequently predicted bottomhole WOB and torque using a linear regression model, they evaluated model performance using the RMSE and selected the gradient boosting algorithm as the optimal approach. However, this method had certain limitations. The model only incorporated inputs such as flow rate while

neglecting strongly correlated physical parameters like well depth and inclination angle, resulting in limited generalization capability. Marquez (2021) developed an XGBoost model for predicting bottomhole torque in shallow water wells in the Gulf of Mexico, although its prediction accuracy achieved an R^2 score of 0.83, this study lacked supplementary evaluation metrics and did not incorporate theoretical constraints, resulting in limited model interpretability and transferability. Elzenary (2023) developed a bottomhole WOB prediction model using support vector machines (SVM) based on data from a high-angle well in North Africa, the model achieved an exceptional R^2 score of 0.99 with only around 1000 training samples. However, the limited dataset size and the lack of systematic evaluation of input parameter correlations resulted in poor generalization capability. Wu et al. (2024) optimized the Back Propagation (BP) and Long Short-Term Memory (LSTM) networks using a genetic algorithm to improve the accuracy of bottomhole WOB prediction, achieving enhanced predictive accuracy with a mean absolute error (MAE) of 0.4. However, this study failed to specify the data sources or applicable well conditions, nor did it incorporate relevant physical constraints, resulting in model interpretability and generalization capability that require further validation.

Some researchers have also focused on integrating physical methods with artificial intelligence, an approach that has emerged as a new interdisciplinary research field. For instance, Negara and Saad (2020) analyzed parameter importance in the ROP equation, used a physical model to select input features, and incorporated these parameters into a machine learning model for ROP prediction. However, their method relied on too few parameters and suffered from insufficient constraints. Li et al. (2025) combined mechanical analysis with machine learning to predict build-up rates. After calculating mechanical parameters such as lateral force, they integrated them as inputs to expand the dataset and enhanced prediction accuracy by modifying the loss function. Nevertheless, their approach has limitations: the mechanical model parameters are difficult to measure accurately in practice, and its applicability in marine environments remains unvalidated. Albattat et al. (2025) simulated mud loss scenarios by adjusting fluid parameters and applied machine learning to predict fracture-induced losses using synthetic data, achieving promising results. Despite this, the study was constrained by limited data availability and practical applicability. Qi et al. (2025) developed a drilling optimization model that integrates physical mechanisms with machine learning. They incorporated mechanical specific energy calculations into the input data and optimized drilling parameters under vibration constraints, demonstrating superior performance. A key limitation, however, is that the model was developed and tested on a single dataset, lacking validation with field data. Similarly. Atheaux et al. (2025) combined spectroscopic analysis with machine learning to analyze mineral elements in drilling fluid, enabling accurate solid content measurement. This method, however, remains confined to laboratory research and has not yet been deployed in field operations.

In summary, although artificial intelligence methods have made a lot of progress in the field of drilling, there are relatively few studies in the field of bottomhole WOB prediction. At present, the existing bottomhole WOB prediction models are primarily data-driven and do not give much consideration to the physical meaning behind the models, resulting in low interpretability, poor generalization capability, and difficulty in capturing the characteristics of long-term changes. Moreover, there is a scarcity of research specifically focused on bottomhole WOB prediction for offshore extended-reach wells.

Therefore, this paper takes the typical extended-reach wells in the South China Sea as the research object. Aiming at the problems such as low accuracy, poor interpretability and generalization ability of the existing pure data-driven models, multiple groups of different bottomhole WOB composite prediction models are established, and the constraints of the ROP equation are integrated into the models to combine the physical equations to the greatest extent. By systematically comparing and verifying the newly established model with other existing prediction models on the new well data, the optimal model is selected, and the sensitivity analysis and interpretability analysis of the input parameters that affect the optimal model are carried out. This approach not only achieves accurate bottomhole WOB prediction for offshore extended-reach wells but also successfully overcomes the inherent limitations of traditional purely data-driven models.

2. Physics theories and intelligent methods

2.1. Rate of penetration equation

The ROP refers to the depth a drill bit advances into the formation within a unit of time, serving as a critical metric for evaluating drilling efficiency (Shaabani et al., 2016). In the actual drilling process, the ROP is influenced by a combination of multiple factors, including the WOB, rotations per minute of drill bit (RPM), hydraulic conditions, and the performance of the drill bit. The ROP equations vary depending on the type of drill bit selected, and there have been studies by various scholars on ROP equations for different types of drill bits (Khoshouei and Bagherpour, 2023). Since PDC bits are generally used for drilling operations in extended-reach offshore drilling, this study primarily considers the relevant ROP equations for PDC bits (Heydari et al., 2017). The following equations were established by Bingham, Hareland, Motahari, and others, which take into account different factors for the ROP equations of PDC bits (Mazen et al., 2021).

Bingham ROP Equation (Bingham, 1965):

$$ROP = \mathrm{a} \times RPM \times \left(\frac{WOB}{D_b}\right)^b \tag{1}$$

in the equation, D_b represents the diameter of the drill bit, while a and b denote the influence coefficients of rock strength.

Hareland ROP Equation (Hareland et al., 2010):

$$\begin{cases} ROP = \dfrac{14.14 \times N_c \times RPM \times A_c}{D_b} \\ A_c = \cos\alpha \sin\theta (N1 - N2) \\ N1 = \left(\dfrac{d_c}{2}\right)^2 \cos^{-1}\left(1 - \dfrac{2DOC}{2\cos\theta \times d_c}\right) \\ N2 = \left(\dfrac{d_c \times DOC}{\cos\theta} - \dfrac{DOC^2}{\cos^2\theta}\right)^{0.5} \left(\dfrac{d_c \times DOC}{2\cos\theta}\right) \end{cases} \tag{2}$$

in the equation, N_c represents the number of cutting teeth, D_b denotes the diameter of the drill bit, A_c stands for the cutting area in front of the cutting teeth, d_c signifies the diameter of the cutting teeth, DOC indicates the depth of cut, α is the side rake angle of the PDC bit's cutting teeth, and θ represents the back rake angle.

Motahari ROP Equation (Motahhari et al., 2010):

$$ROP = W_f \times \left(\frac{G \times RPM^x \times WOB^y}{D_b \times S}\right) \tag{3}$$

in the equation, G represents the coefficient calculated from the bit geometry and the size of the cutting teeth, W_f denotes the bit wear function, x and y signify the exponents that influence the ROP

model, and S stands for the confined rock strength.

2.2. Convolutional neural networks

Depending on the type of problem to be solved, convolutional neural networks (CNN) can transform the input data structure into the required structure type through dimensional changes, mainly including one-dimensional, two-dimensional, three-dimensional and other different structures. Among them, one-dimensional convolutional networks are primarily used for processing sequential data, while two-dimensional convolutional networks and three-dimensional convolutional networks are used to process dimensional changes (Alzubaidi et al., 2021; Zhou et al., 2017). Typically, a convolutional structure is composed of convolutional layers, pooling layers, and fully connected layers (Krizhevsky et al., 2017). The convolutional layer extracts local features from the input data, the pooling layer reduces computational complexity, and the fully connected layer produces the final output. Between the convolutional and pooling layers, activation functions are typically applied to enhance the model's expressive power and mitigate issues such as underfitting.

2.3. LSTM memory networks

LSTM networks can make up for the drawback that traditional recurrent neural networks have a limited ability to capture temporal and sequential data (Sutskever et al., 2014). When dealing with such problems, the LSTM processes sequential data through iterative time steps. Its gates selectively filter information, updating the cell state by forgetting irrelevant data and incorporating new inputs, thereby propagating only the most relevant information forward. Therefore, the LSTM structure can effectively solve the prediction problems of long sequence and temporal data, and can alleviate the problem of gradient explosion and vanishing (Chen et al., 2024). As illustrated in Fig. 1, the LSTM unit structure centers on three gating mechanisms: the forget gate, input gate, and output gate. The relevant calculation equations are shown as Equation (4) (Graves and Schmidhuber, 2005).

$$\left\{\begin{array}{l} i_t = \sigma(W_i[x_t, h_{t-1}] + b_i) \\ f_t = \sigma\left(W_f[x_t, h_{t-1}] + b_f\right) \\ o_t = \sigma(W_o[x_t, h_{t-1}] + b_o) \end{array}\right\} \tag{4}$$

in the equations, x_t denotes the current input feature and h_{t-1} represents the previous hidden state, σ represents the activation function; i_t, W_i, and b_i denote the output, weight matrix, and bias term of the input gate, respectively; f_t, W_f, and b_f represent the output, weight matrix, and bias term of the forget gate, respectively; o_t, W_o, and b_o signify the output, weight matrix, and bias term of the output gate, respectively.

Bidirectional Long Short-Term Memory (Bi-LSTM) is an extension of the standard LSTM architecture, incorporating both forward and backward LSTM layers (Chen et al., 2024). This dual structure enables each cell to utilize information from both past and future hidden states, thereby capturing richer contextual features and achieving higher stability (Greff et al., 2016).

2.4. Transformer method

The Transformer model was initially proposed by Vaswani et al. (2017) to better capture dependencies between elements in a sequence. As shown in Fig. 2, the model's core unit consists of an Encoder and a Decoder (Liu et al., 2021). Furthermore, internally, both components are constructed from a looped stack of identical sub-layers, including multi-head self-attention mechanisms, Add & Norm operations, and position-wise feedforward networks. This structure provides a key architectural advantage in parallelizability over recurrent models like Recurrent Neural Networks (RNNs), as unlike their sequential data processing method, the Transformer processes all elements simultaneously, significantly reducing computation time.

The self-attention mechanism is the core of the Transformer model, designed to enable the model to focus on the correlations between different parts of the entire input elements (Kang and McAuley, 2018). Specifically, in this process, the input is linearly projected into three matrices: Query (Q), Key (K), and Value (V). These matrices are then used to dynamically compute attention

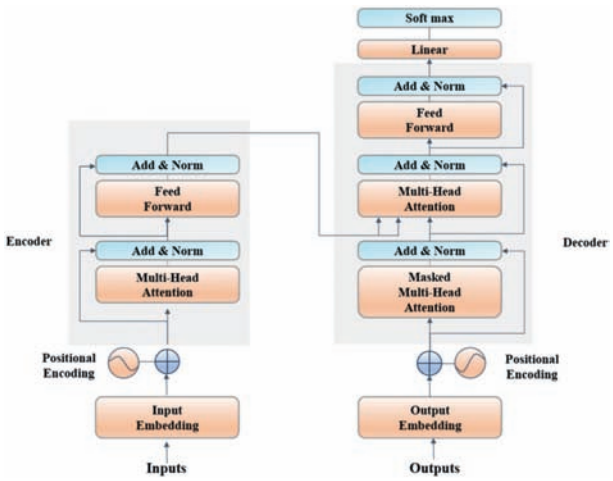


Fig. 2. Transformer architecture.

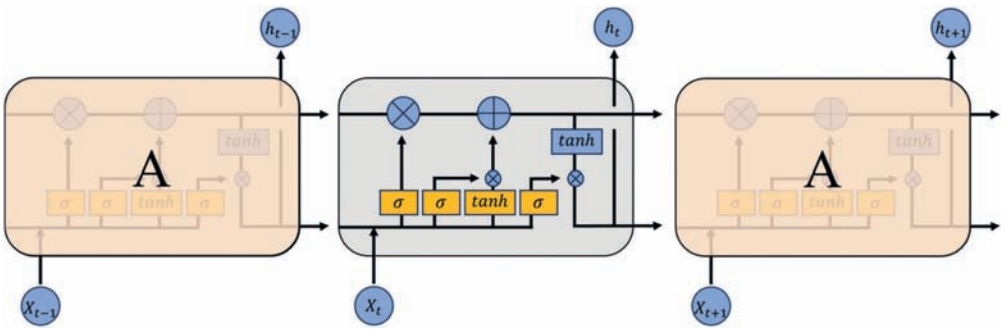


Fig. 1. LSTM structure diagram.

weights, allowing the self-attention mechanism to effectively capture dependencies (Maurício et al., 2023). The equation for this is expressed as follows:

$$Attention(Q,K,V)=\text{Softmax}\left(\frac{QK^T}{\sqrt{d}}\right)\text{V} \tag{5}$$

In the equation, Q, K, and V represent the Query matrix, Key matrix, and Value matrix, respectively.

3. Data processing and intelligent model structure design

3.1. Data processing

This study selects data from three extended-reach wells (Well A, Well B, and Well C) in a complex deepwater block in the South China Sea. The dataset includes 13 features, such as well depth, bottomhole WOB, weight on hook (WOH), torque, RPM, ROP, flow rate, bit time, pump time, standpipe pressure (SPP), Inclination (Inc), Azimuth (Azi), and mud density, totaling over 800,000 data points. Table 1 shows the parameter ranges for the three wells. Due to interference from external environmental factors such as variations in temperature and pressure, combined with complex geological and wellbore conditions, the acquired raw data exhibit substantial noise and outliers. This makes the data unsuitable for direct use as model inputs. Therefore, the original data require preprocessing and noise reduction before model development.

Firstly, the original data need to be processed for duplicate values, missing values and outliers. Since the volume of the original data is large, both duplicate values and outliers are directly deleted. For missing values, the random forest filling method is adopted for data filling. Then, noise reduction processing is carried out. In this study, a data noise reduction method combining Gaussian filtering and wavelet transform is used. Due to the characteristics of Gaussian filter weight distribution, it assigns less weight to the data boundaries and small amplitude anomaly points, avoiding excessive interference with these points and ensuring data integrity with overall smoothness characteristics (An et al., 2015; Pan et al., 2022). In this study, a standard deviation (σ) of 1 was adopted for the Gaussian filter, thereby preserving the majority of underlying trends and critical features. The wavelet transform then processes this smoothed data at different dimensions, analyzing it from both frequency and time windows, achieving multi-scale transformation of the data and thus processing the noise points. Finally, the inverse transform is performed through soft thresholding to obtain the denoised data. This combined methodology effectively enhances the signal-to-noise ratio while preserving critical details.

$$W(x,y)=\frac{1}{\sqrt{|x|}}\int_{-\infty}^{+\infty}f(t)\varphi\left(\frac{t-y}{x}\right)dt \tag{6}$$

As shown in Equation (6), which represents the wavelet transform equation, x and y are the two scales of the wavelet transform, controlling the scaling and translation of the wavelet function φ, respectively, and t is the sliding window of the time step. This study selects a Gaussian filter kernel with a standard deviation of 1, uses the biorthogonal 'bior3.5' wavelet basis, extracts the second layer of decomposition results, and applies the soft thresholding method to obtain the final denoised data. As can be seen from Fig. 3, the denoised data effectively eliminates most typical noises. Its change curve becomes significantly smoother, while retaining the main features of the original data and maintaining a high degree of consistency with the trend of the original data, which can provide a reliable data basis for the subsequent analysis.

Table 1
Partial parameter range table.

Parameter range	Well A	Well B	Well C
Depth (m)	845–4096	1027–4267	997–4101
Inc(°)	1.93–87.43	2.05–88.14	1.75–87.2
SPP(psi)	396–3248	242–3948	442–3914
ROP(m/h)	1.07–165.54	0.58–151.47	2.33–180.7
Torque (klbf.ft)	2.56–22.24	2.42–18.81	2.38–17.93
Bottomhole WOB(klbs)	1.6–21.05	2.04–15.75	2.18–18.4

The next step is to conduct a correlation analysis. Since the bottomhole WOB can be considered, to some extent, as sequential data that varies with well depth, this study adopts the Spearman correlation coefficient, which is suitable for ordinal data. The Spearman correlation coefficient ranges from [−1, 1]. A value closer to 1 indicates a stronger positive correlation between the parameters, while a value closer to −1 indicates a stronger negative correlation. When the coefficient is close to 0, it suggests a very low correlation between the parameters. The heatmap of correlation analysis for Well A is illustrated in Fig. 4.

From the correlation comparison images, it can be deduced that most of the collected data are positively correlated with the bottomhole WOB, while the bottomhole WOB is negatively correlated with the ROP, flow rate and Azi. The correlation coefficient between pump time and bottomhole WOB is less than 0.3, however, pump time has a strong relationship with other parameters, suggesting that pump time indirectly affects changes in bottomhole WOB through its influence on other parameters and should not be entirely excluded. After comprehensive consideration, it is concluded that all selected parameters can serve as input parameters for the predictive model. After data denoising, a standardization process is applied to transform the input data into a normal distribution with a mean of 0 and a standard deviation of 1, in order to eliminate the influence of different units of measurement among the input parameters (Krizhevsky et al., 2017). For the division of model input data, this study constructs the training, validation, and test sets as follows: first, data from the same depth intervals of Well A and Well B are merged and uniformly preprocessed to form the input dataset. From this dataset, the first 70% of the data sorted by depth is used as the training set, and the remaining 30% serves as the validation set. The complete data from Well C is used as the test set for model evaluation.

The process studied in this study is shown in Fig. 5 as follows. Firstly, the drilling parameters are preprocessed, including operations such as data cleaning, data denoising, and correlation analysis. Subsequently, multiple prediction models are established, including both the existing traditional prediction models and the new model combining the mechanism established in this study. Hyperparameter tuning is performed on these models to obtain the best model. The third step involves dividing the processed data and substituting it into the model for prediction and evaluation to verify the applicability of the newly established model. Finally, an interpretability analysis is conducted on the model with the best performance to analyze the influence degree of each parameter on the model results.

3.2. CNN-BiLSTM model

This section establishes a Convolutional-Bidirectional Long Short-Term Memory Neural Network (CNN-BiLSTM) model for predicting bottomhole WOB. The model sequentially combines a CNN with a BiLSTM network. Specifically, as shown in Fig. 6, the architecture and prediction process proceed as follows: firstly, the

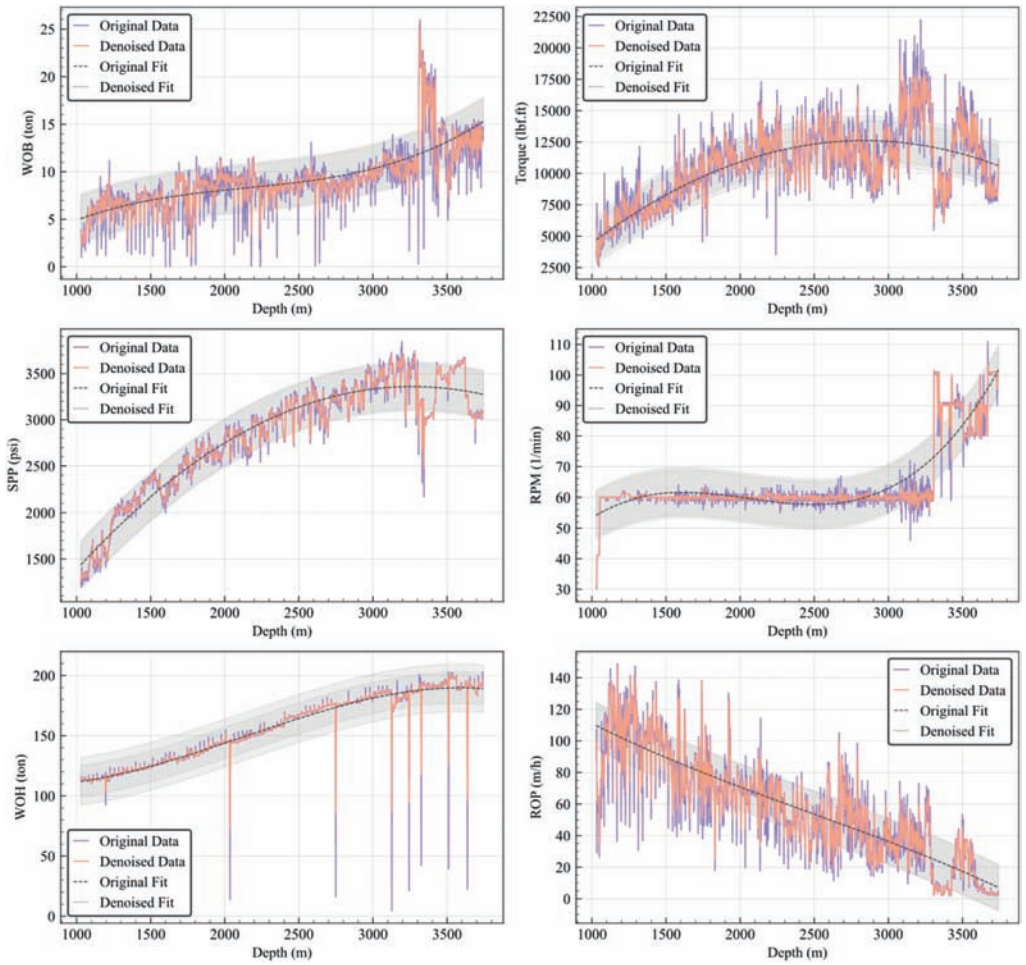


Fig. 3. Comparison of partial data before and after denoising (using well a as an example).

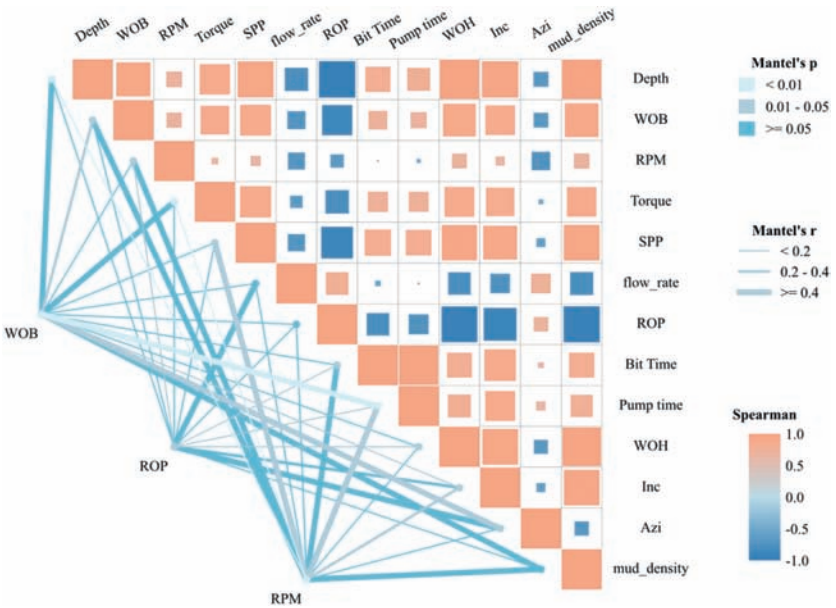


Fig. 4. Correlation heatmap (using well a as an example).

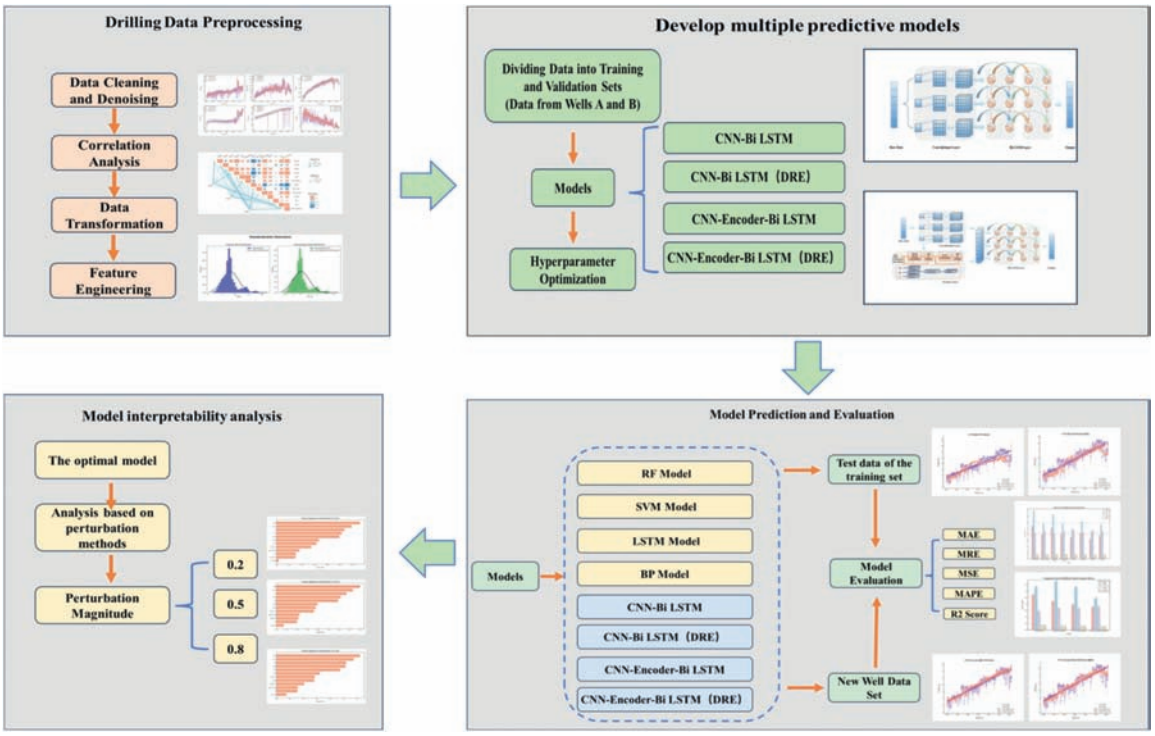


Fig. 5. Workflow diagram.

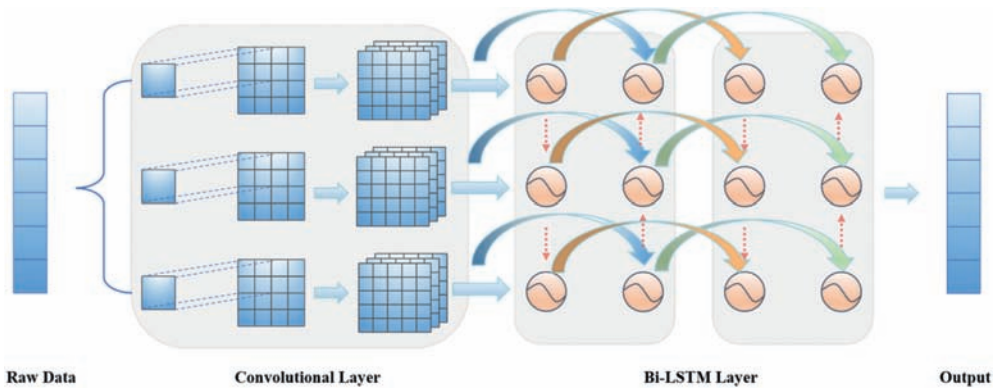


Fig. 6. CNN-BiLSTM network architecture.

processed data is transformed through convolution and other operations into a higher-dimensional representation to meet the input format requirements of the BiLSTM network. The second step is to input the transformed data sequence into the BiLSTM network to extract the association information and hidden features between adjacent data within each window. Finally, the final prediction result is output through the feedforward neural network (FNN). Next, the PSO algorithm is employed to identify the optimal hyperparameters for the established CNN-BiLSTM model. After continuous tuning, the selected hyperparameters of the final model are listed in Table 2.

Table 2
Internal hyperparameters of the CNN-BiLSTM network.

Model Parameters	Value
Number of channels in Convolutional Layer 1	32
Number of channels in Convolutional Layer 2	91
Number of channels in Convolutional Layer 3	50
LSTM Hidden Layer Size	138
Number of LSTM Layers	3
Dropout Rate	0.2
Batch size	20
Sequence Length	8
Number of Training Epochs	94
Learning Rate	0.0028

3.3. CNN-encoder-BiLSTM model

This section establishes a Convolutional-Encoder-Bidirectional Long Short-Term Memory fusion neural network model (CNN-Encoder-BiLSTM). Since the prediction of bottomhole WOB outputs continuous values, which is a regression problem, there is no need for specific decoding in the output. Therefore, the composite model structure does not require the Decoder module of the Transformer. As shown in Fig. 7, the structure and prediction process of the model is presented: The framework consists of a CNN-Encoder for

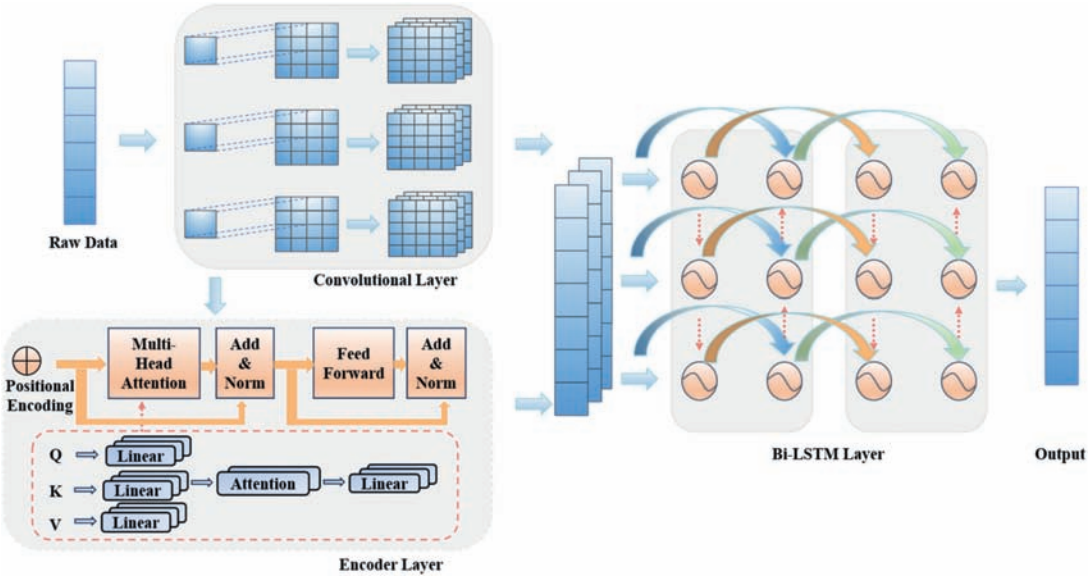


Fig. 7. CNN-encoder-BiLSTM network architecture.

feature extraction and a BiLSTM module that acts as the decoder. In the CNN-Encoder module, on the one hand, the input parameters undergo dimension changes through the one-dimensional convolutional network structure to expand the data and increase the dimension. On the other hand, the data after partial CNN operations is encoded through the Encoder layer to locate each feature. Next, the two sets of data are merged. Finally, the output features are passed into the BiLSTM network to identify the interrelationships among the data within each window, and then undergo dimension reduction to output the prediction result. Subsequently, the PSO optimization algorithm was employed to fine-tune the model's hyperparameters. After optimization, the key parameters of the constructed hybrid model are presented in Table 3.

3.4. Design of composite model constrained by rate of penetration equation

To enhance the prediction accuracy and interpretability of the model, theoretically, establishing an appropriate loss function is one of the feasible approaches. Therefore, the method adopted in this study involves introducing a ROP constraint into the original loss function. From Equations (1)–(3), it can be concluded that the ROP equation is generally proportional to the bottomhole WOB and RPM. Since in field operations, bit wear changes are difficult to measure, and various constraint coefficients require extensive computation, consuming significant time and resources, this study selects partial equation parameters to flexibly adapt to the construction of the loss function, using $RPM \cdot WOB^x$ as the loss function unit for input.

Table 3
Hyperparameters of the CNN-encoder-BiLSTM network.

Model Parameters	Value
Number of channels in Convolutional Layer 1	30
Number of channels in Convolutional Layer 2	48
Encoder Layer Dimension	48
Number of Attention Heads	8
Number of Encoder Layers	2
LSTM Hidden Layer Size	150
Number of LSTM Layers	3
Number of Training Epochs	21
Dropout Rate	0.2
Learning Rate	0.0019
Batch Size	20
Sequence Length	8

The calculation method for the custom loss function within each computation window is shown in Equation (7). Specifically, for the Mean Squared Error (MSE) calculated within any step window, the variation error of the computed N value within the window is added. If the error exceeds a set threshold, it indicates that the predicted bottomhole WOB value at this window node is significantly incorrect, representing a larger deviation from the true value. Therefore, the calculated variation error is multiplied by a coefficient pf to enable the model to learn the hidden features within the current window and thereby reduce the error magnitude. For data where the error is below the set threshold, it indicates that the predicted bottomhole WOB value at this window node is close to the true bottomhole WOB value, and thus the pf coefficient is set to 1. Subsequently, the computed variation error of the N value within the window is multiplied by a relevant weighting coefficient to ensure the overall stability of the model.

$$
\begin{aligned}
&ROP \propto RPM \cdot WOB^x \\
&N = \frac{ROP}{RPM \cdot WOB^x} \\
&pf = \begin{cases} \mathrm{m} & \left|N_{true} - N_{pred}\right| > threshold \\ 1 & \left|N_{true} - N_{pred}\right| \le threshold \end{cases} \\
&delatN = pf \cdot \frac{\left(N_{true} - N_{pred}\right)}{N_{true}} \\
&MSE_{data} = \frac{1}{\mathrm{n}} \sum_{i=1}^{n} \left(N_{true} - N_{pred}\right) \\
&MSE_{delatN} = \frac{\partial f}{\partial delatN} \\
&LOSS = \lambda_1 \cdot MSE_{data} + \lambda_2 \cdot MSE_{delatN}
\end{aligned}
\tag{7}
$$

in the equation, N represents the ratio of $RPM \cdot WOB^x$, serving as a newly added physical constraint factor in the custom loss function.

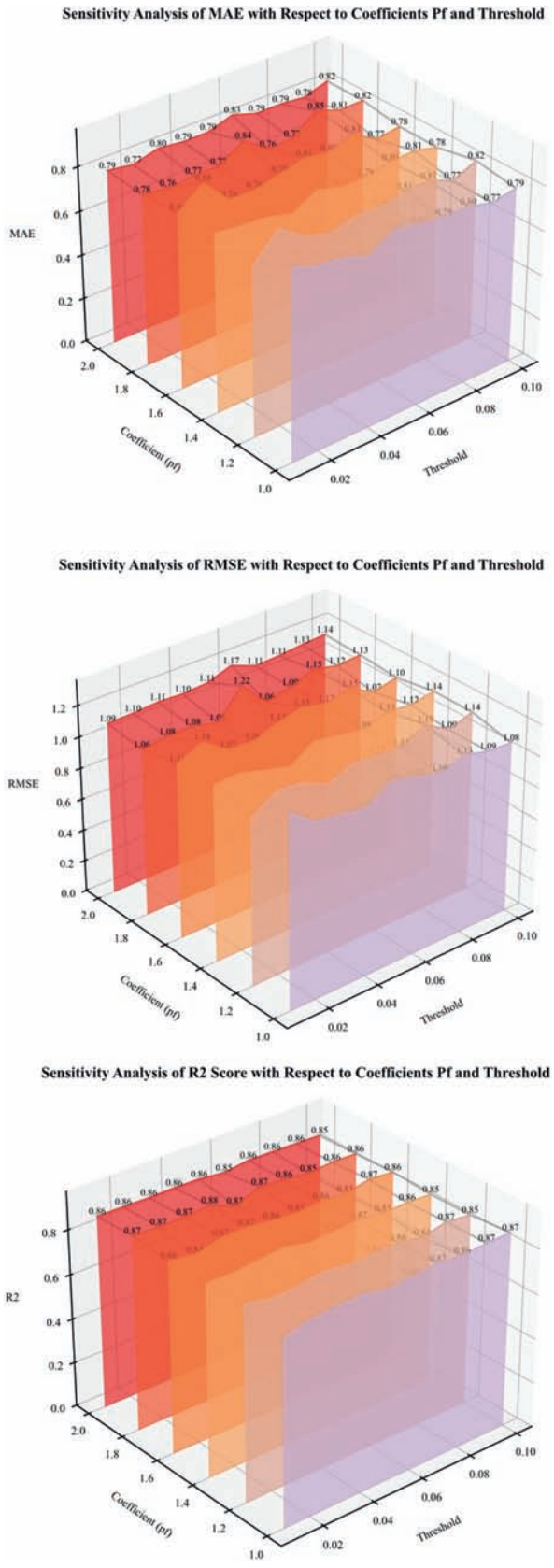


Fig. 8. Comparison chart of sensitivity analysis.

N_{true} and N_{pred} denote the constraint factor values calculated based on the actual and predicted bottomhole WOB, respectively.

By replacing the original loss functions of the two models with the newly established loss function, the corresponding Rate of Penetration equation-constrained models are obtained: the CNN-BiLSTM(DRE) model and the CNN-Encoder-BiLSTM(DRE) model, where DRE represents a custom loss function term incorporating the ROP equation constraint. Subsequently, sensitivity analysis was performed on the models with different *pf* values and threshold values to obtain the optimal model. Fig. 8 shows the parameter comparison chart after the sensitivity analysis, from which it can be concluded that the optimal *threshold* value is 0.04 after sensitivity analysis, and when $\left|N_{true} - N_{pred}\right| > threshold$, the optimal *pf* value is 1.4.

4. Model evaluation criteria and result

4.1. Model evaluation criteria

Since this study focuses on the prediction of bottomhole WOB, a regression problem characterized by continuous variables. Therefore, in this paper, MAE, Mean Relative Error (MRE), MSE, MAPE, R^2 are selected as the model evaluation indicators. The smaller the MAE, MRE, MSE and MAPE are, the greater the prediction accuracy of the model is. The larger the R^2 is, the higher the degree of model fitting is indicated.

4.2. Model results

According to Section 3 of the paper, we established four primary models: the CNN-BiLSTM model, CNN-Encoder-BiLSTM model, and their enhanced versions incorporating the rate of penetration equation loss function - CNN-BiLSTM(DRE) and CNN-Encoder-BiLSTM(DRE). For comparative evaluation, we also implemented several benchmark models including a SVR model with Radial Basis Function (RBF) kernel function, a RF model configured with 100 decision trees and a maximum depth of 10, a BP Neural Network model featuring a five-layer architecture with neuron counts of 200, 100, 50, 25, and 1 respectively, and a baseline LSTM model with 150 hidden units and 3 layers. Table 4 present the comparative results of bottomhole WOB predictions and evaluation metrics for each model using test data from the training wells (Wells A and B). The data partitioning scheme is identical to that described in the previous chapter, with 70% used for model training and 30% reserved for testing and evaluation. Fig. 9 shows that all models achieve high consistency between predicted and actual bottomhole WOB values, with predicted trends closely matching the actual variations along well depth. Fig. 10 presents a comparative analysis of all models across

Table 4
Performance evaluation table of different models on the known data test set.

Model	MAE	MRE	MSE	MAPE	R2 score
CNN-BiLSTM Model	1.07	0.131	1.581	12.4%	0.814
CNN-Encoder-BiLSTM Model	0.788	0.104	1.145	10.3%	0.871
CNN-BiLSTM(DRE)Model	1.00	0.125	1.458	12.3%	0.821
CNN-Encoder-BiLSTM(DRE)Model	0.787	0.104	1.144	10.4%	0.872
BP Network Model	0.823	0.102	1.137	10.1%	0.858
LSTM Model	0.832	0.110	1.221	11.0%	0.834
RF Model	0.633	0.087	0.861	8.6%	0.921
SVR Model	0.742	0.101	1.107	10.1%	0.873

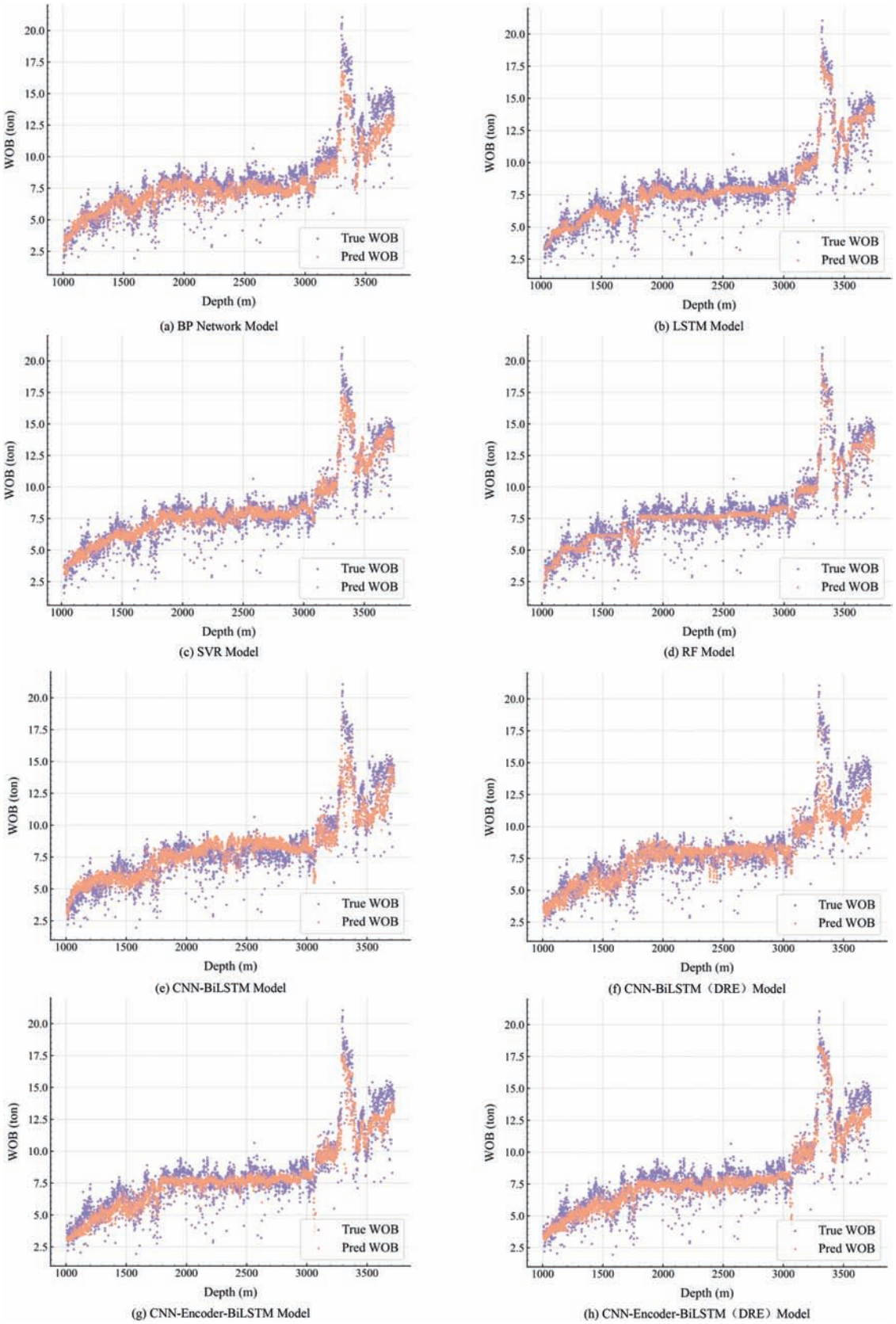


Fig. 9. Comparison of actual and predicted bottomhole WOB on the complete Well-A dataset.

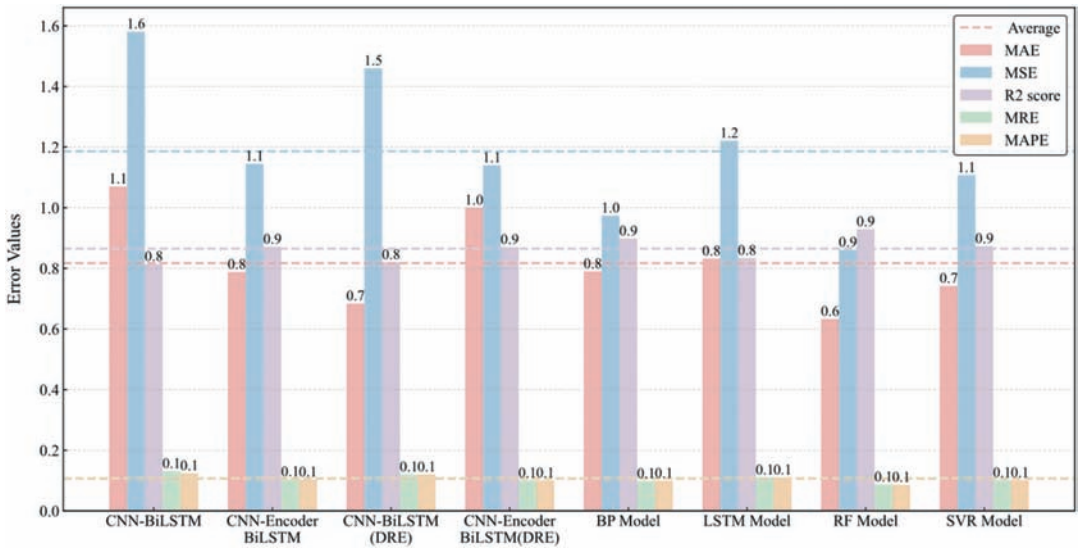


Fig. 10. Comparison chart of performance evaluation of different models on the known data test set.

different evaluation metrics, demonstrating that each model exhibits generally consistent performance in terms of MRE, MAPE, and other indicators, all maintaining good fitting capability. However, validation solely on training well test data remains insufficient for determining the most suitable model for bottomhole WOB prediction. Therefore, comprehensive testing of all models on completely unknown wells within the same depth range is necessary to further evaluate their respective performances.

As shown in Fig. 11, the curves depict the variation relationship between the predicted bottomhole WOB values and the actual values for four newly established models and four other commonly used models in the new well (Well C). It is evident from the figure that, compared to conventional prediction models, the four newly developed composite models exhibit a close alignment between the predicted bottomhole WOB and the actual values. Additionally, the figure illustrates the degree of fit between the trend lines of the predicted values from the four new models and the trend lines of the actual values.

Fig. 12 and Table 5 provide a comprehensive performance evaluation of the four newly developed models. Comparative analysis demonstrates that models incorporating Transformer's Encoder module exhibit superior performance across all metrics when benchmarked against the CNN-BiLSTM model. The integration of ROP equation-based loss function further enhances the performance of all baseline models, with the CNN-Encoder-BiLSTM (DRE) variant showing particularly remarkable improvement and achieving the best overall performance. Quantitative comparisons show that compared to the original CNN-BiLSTM and the original CNN-Encoder-BiLSTM models, the proposed model achieves reductions in MAE by 36% and 10%, in MRE by 30% and 19%, in MSE by 27% and 26%, and in MAPE by 29% and 11%, respectively, along with improvements in R^2 score by 24% and 7%.

As shown in Fig. 13 and Table 6, ROP, Torque, Azi, RPM, and SPP consistently rank as the five most influential features on the model output, with contributions significantly higher than those of other parameters. Among these, ROP is the most prominent feature, ranking first in importance. RPM, as one of the key variables incorporated into the custom loss function, also stably remains among the top five features. Moreover, as the perturbation level increases, the importance of RPM shows a pronounced upward trend, reflecting the model's growing sensitivity to this parameter. Specifically, as perturbation amplitude increases, the incremental importance of ROP decreases from 0.047 to 0.041. The importance difference between ROP and Torque shows a non-monotonic trend (first rising then declining). The importance differences between ROP and SPP and between ROP and RPM exhibit continuous increases at diminishing rates. Torque and Azi rank as the second and third most important features, respectively. The importance of Torque grows steadily with perturbation. The incremental importance of Azi declines from 0.039 to 0.036. The importance of SPP strengthens with perturbation, with its incremental importance dropping from 0.033 to 0.029.

5. Discussion

5.1. Model discussion and engineering value

Based on the results from Section 4 (Figs. 10 and 12, Tables 4 and 5) and the performance of the optimal CNN-Encoder-BiLSTM (DRE) model, the main findings are presented.

First, the composite model effectively integrates the advantages of individual models and demonstrates stable predictive performance across diverse datasets. In contrast, although single models such as BP, LSTM, RF, and SVR perform well on known test sets, their accuracy decreases significantly when applied to new well data, failing to capture the actual variation trends of bottomhole WOB. This phenomenon reveals the inherent shortcoming of excessive reliance on training data in single models. By leveraging its integrated structure, the composite model ensures reliable prediction trends without significant anomalies.

Furthermore, the incorporation of a physics-constrained loss function enhances both predictive accuracy and physical plausibility. As shown in the 2500–3500 m interval in Fig. 11, predictions from the model without physical constraints exhibit an overly smooth, nearly linear distribution, deviating from actual conditions. In contrast, with the physics-constrained loss function, the predictions not only achieve higher accuracy but also display fluctuations closer to real measurements, confirming the corrective and interpretative role of physical constraints in refining model predictions.

In summary, the CNN-Encoder-BiLSTM(DRE) hybrid model proposed in this study holds significant engineering application value in practical drilling operations. The model can be trained

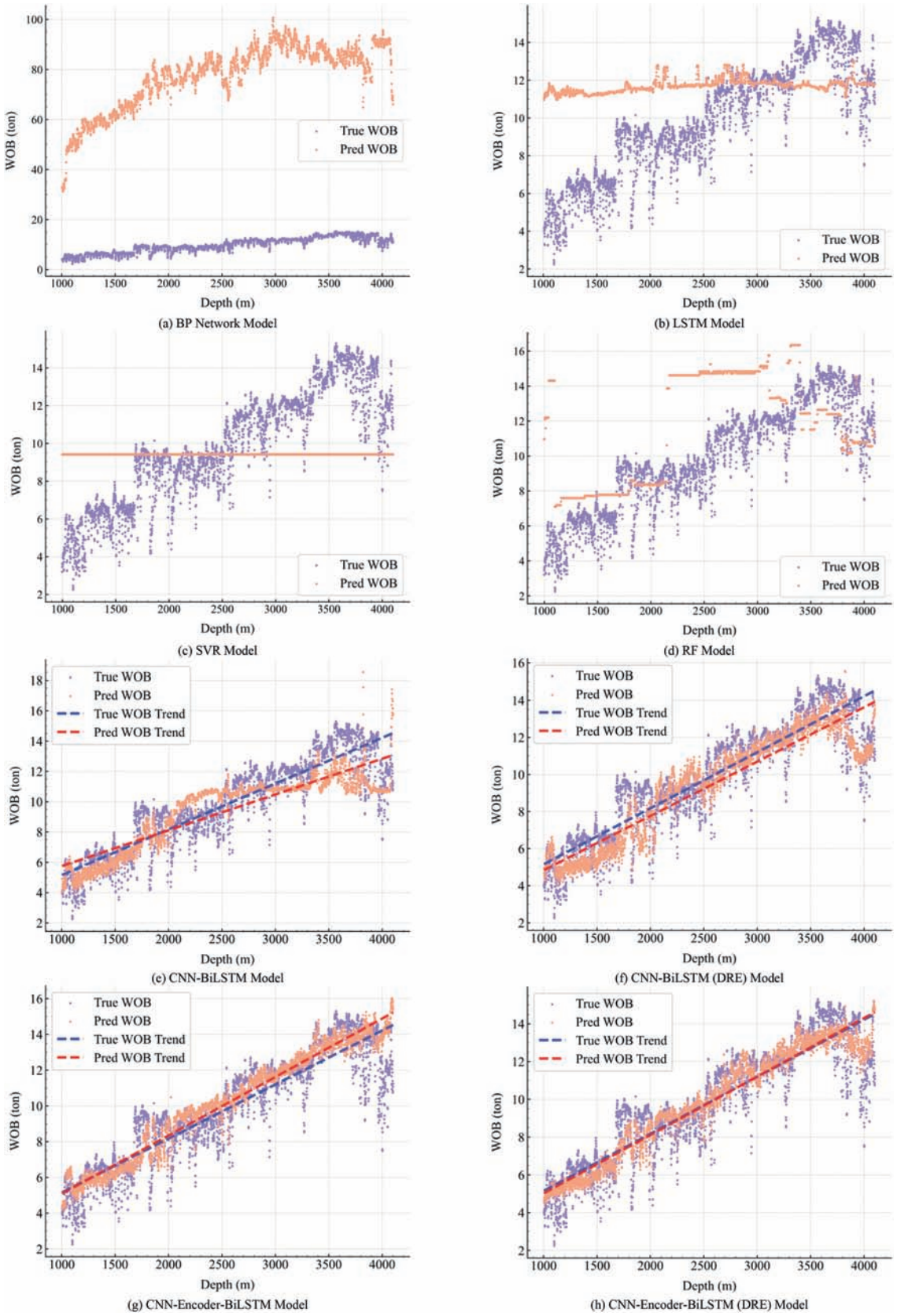


Fig. 11. Comparison of the actual bottomhole WOB of the new well (Well C) with the predicted bottomhole WOB.

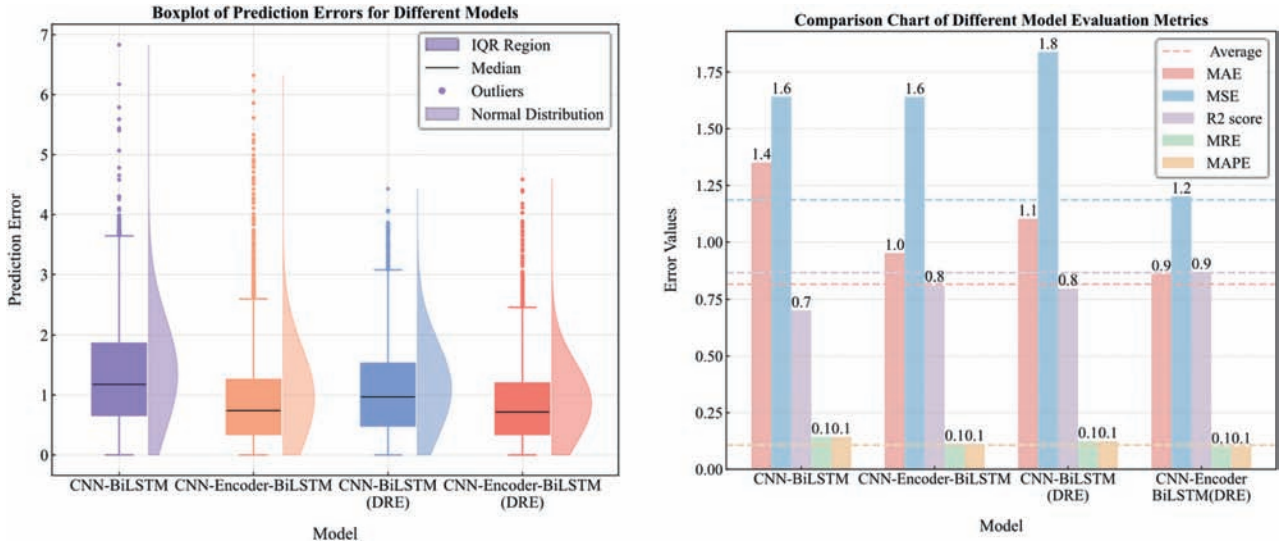


Fig. 12. Error comparison of different prediction models.

Table 5
Performance Evaluation Tables for newly established Different Models.

Models	MAE	MRE	MSE	MAPE	R2 score
CNN-BiLSTM Model	1.351	0.143	1.641	14.3%	0.701
CNN-Encoder-BiLSTM Model	0.951	0.112	1.640	11.2%	0.812
CNN-BiLSTM (DRE) Model	1.103	0.124	1.838	12.4%	0.797
CNN-Encoder-BiLSTM (DRE) Model	0.859	0.100	1.201	10.0%	0.867

using data from offset wells or existing wells within the same block, enabling high-precision prediction of bottomhole WOB with strong trend consistency for new target wells. It provides critical data support for field personnel to monitor downhole conditions—such as abnormal vibrations, bit wear, and lithological characteristics—through predicted bottomhole WOB values and their dynamic variations. This capability offers the potential to achieve early risk diagnosis and adaptive optimization of drilling parameters.

5.2. Feature importance analysis

Through analysis of the changes in the top five important features of the model under varying perturbation levels in Table 6, the following content was revealed.

Specifically, ROP serves as the most important feature, directly reflecting the interaction between bottomhole WOB and the formation. As the perturbation amplitude increases, the growth rate of its importance slows down. Torque, which directly reflects bit cutting resistance and downhole friction, exhibits a strong correlation with bottomhole WOB, and its importance rises with increasing perturbation intensity. Although Azi lacks a direct physical relationship, its significance may stem from its joint role with Inc in characterizing formation properties and wellbore trajectory, thereby indirectly influencing predictions. Its gradual importance growth suggests that it functions more as a model constraint rather than a direct driver of outcome changes. As a hydraulic parameter, SPP reflects wellbore cleaning and circulatory system stability, indirectly affecting mechanical parameters such as bottomhole WOB. While its importance continues to strengthen, the growth rate decelerates, indicating a trend toward stabilization in its contribution. In contrast, the importance of RPM shows an accelerating upward trend, demonstrating a sustained and significant increase in the model's sensitivity to this parameter.

The analysis of the importance changes in ROP and RPM reveals a divergence in feature significance. This phenomenon is consistent with the design concept of the custom loss function: by incorporating physical constraints among ROP, RPM, and the predicted values, the loss function dynamically adjusts the weights of these parameters during inference, guiding the model to learn the relationship between them rather than relying solely on independent statistical patterns. As perturbation intensifies, the importance of RPM increases at an accelerating rate, indicating that when input data deviates from the training distribution, the model tends to rely more on the patterns jointly represented by ROP and RPM. By adhering to the custom constraints, the model maintains the rationality of its predictions.

In summary, the introduction of a physics-constrained loss function enables the model to go beyond the parameter learning approach confined to statistical correlations in purely data-driven methods, allowing it to capture the actual interaction mechanisms among parameters, thereby enhancing both the reliability and interpretability of the model. In drilling engineering, integrating physical equations among parameters into intelligent learning can provide a theoretical basis for drilling parameter prediction, optimization, and risk identification.

5.3. Research limitations

Through the analysis of the predictive model and parameter importance evaluation, although this study has certain contributions, it still has some limitations. In terms of input data, due to the lack of detailed geological data, the model did not fully learn knowledge related to geological conditions, which has a certain impact on generalizability. In addition, through the analysis of the loss function and changes in input parameter importance, the currently introduced physical constraints are insufficient: the ability to represent relevant formulas such as the hydraulic equation represented by SPP and drilling fluid properties is weak.

6. Conclusion and future work

This study addresses the challenge of predicting bottomhole WOB in offshore extended-reach drilling by proposing a composite

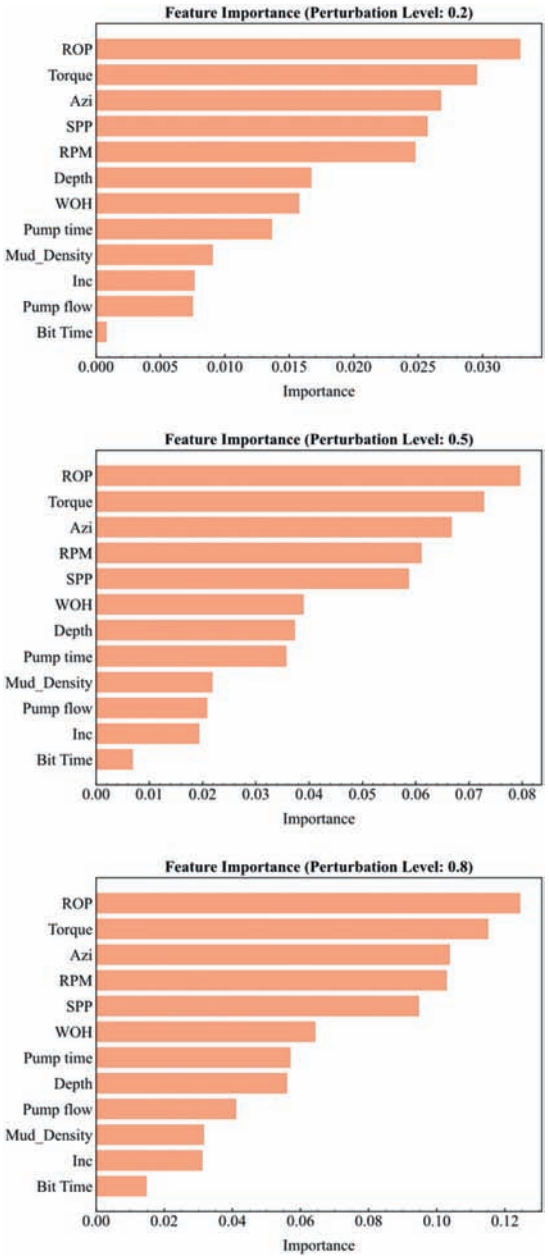


Fig. 13. The influence magnitudes of input parameters under different perturbation amplitudes.

Table 6
Influence rankings of the top five parameters under different perturbation amplitudes.

Feature	Level = 0.2	Level = 0.5	Level = 0.8
ROP	0.0328	0.0798	0.1211
Torque	0.0291	0.0731	0.1191
Azi	0.0263	0.0653	0.1012
SPP	0.0245	0.0579	0.0869
RPM	0.0237	0.0617	0.101

modeling approach that integrates physical constraints. The following conclusions can be drawn.

(1) The composite model integrating the Transformer Encoder with CNN-BiLSTM demonstrates superior performance, exhibiting significant improvements in both prediction accuracy and generalization capability compared to conventional models.

(2) By incorporating the ROP equation as a physical constraint into the loss function, a new loss function (DRE) is constructed, which effectively enhances the model's accuracy and stability. Interpretability analysis reveals that the CNN-Encoder-BiLSTM (DRE) model appropriately captures the coupling effect between ROP and RPM, thereby verifying its interpretability at a mechanistic level.

(3) Among all evaluated models, the CNN-Encoder-BiLSTM (DRE) model delivers optimal performance for predicting bottomhole WOB, with the following metrics: MAE = 0.859, MRE = 0.100, MAPE = 10.0%, MSE = 1.201, and R^2 = 0.867. Owing to its high predictive accuracy, the model provides reliable support for practical applications such as bit wear monitoring, downhole risk identification, and drilling parameter optimization, underscoring its substantial practical value. Furthermore, the proposed modeling framework can be extended to the prediction and optimization of other drilling parameters, offering valuable insights for broader drilling engineering applications.

For subsequent research, this work will focus on the deep integration of mechanistic models, geological constraints, and deep learning models. Specific directions include, but are not limited to: further optimization of the loss function, structural adjustments of the model, and synergistic combinations of input parameters.

CRediT authorship contribution statement

Shuohang Xue: Writing – original draft, Visualization. **Yanan Geng:** Data curation, Conceptualization. **Xuyue Chen:** Funding acquisition, Formal analysis. **Yi Wu:** Methodology, Funding acquisition. **Changsuo Zhou:** Project administration, Investigation. **Bingxuan Li:** Resources, Methodology. **Pengbo Li:** Visualization, Validation.

Declaration of competing interest

The authors declare that they have no known competing financial interests or personal relationships that could have appeared to influence the work reported in this paper.

Acknowledgments

The authors gratefully acknowledge the supports of the National Natural Science Foundation of China (grant number: U24B2031; 52174012; 52394250; 52394255; 52234002; U22B20126; 51804322), and The "14th Five-Year Plan" Major Science and Technology Project of CNOOC: "Research on Intelligent Drilling Downhole Data Monitoring and Transmission Technology" (grant number: KJGG-2023-15-0201).

References

Abahusayn, M., Foster, B., Brink, J., Kuck, M., 2012. Nikaitchuq extended-reach drilling: designing for success on the north slope of Alaska. SPE Drill. Complet. 27 (4), 501–515.

Abbas, A.K., Alsaba, M.T., Al Dushaishi, M.F., 2022. Comprehensive experimental investigation of hole cleaning performance in horizontal wells including the effects of drill string eccentricity, pipe rotation, and cuttings size. J. Energy Resour. Technol. 144 (6), 063006.

Albattat, R., He, X., Hoteit, H., 2025. Integrated machine learning and analytical modeling for real-time lost circulation in fractured formations. SPE J. 2025, 1–18.

Alsaihati, A., Ismail, M., Elkatatny, S., 2025. Optimization of drilling parameters while drilling surface holes using machine learning and differential evolution. SPE J. 2025, 1–14.
Alum, M.A., Egbon, F., 2011. Semi-analytical models on the effect of drilling fluid properties on rate of penetration (ROP). In: SPE Nigeria Annual International Conference and Exhibition. SPE-150806-MS.
Alzubaidi, F., Mostaghimi, P., Swietojanski, P., Clark, S.R., Armstrong, R.T., 2021. Automated lithology classification from drill core images using convolutional neural networks. J. Petrol. Sci. Eng. 197, 107933.
An, D., Kim, N.H., Choi, J.H., 2015. Practical options for selecting data-driven or physics-based prognostics algorithms with reviews. Reliab. Eng. Syst. Saf. 133, 223–236.
Atashnezhad, A., Akhtarmanesh, S., Sleeper, S., 2020. Rate of penetration (ROP) model for PDC drill bits based on cutter rock interaction. In: ARMA US Rock Mechanics/Geomechanics Symposium. ARMA-2020-1699.
Atheaux, I., Hughes, T.L., Peng, J., Johnson, C.E., Yarman, C.E., Medvedev, A., Makarychev-Mikhailov, S., 2025. XRF-FTIR data fusion and machine learning models for mineralogical analysis of solid mineral mixtures and solid dispersions in drilling fluids. In: SPE/IADC Drilling Conference and Exhibition.
Bilim, N., Karakaya, E., 2021. Penetration rate prediction models for core drilling. Min. Metall. Explorat. 38 (1), 359–366.
Bingham, M.G., 1965. A New Approach to Interpreting—Rock Drillability. Petroleum Pub Co., Tulsa, OK, USA.
Boukredera, F.S., Youcefi, M.R., Hadjadj, A., Ezenkwu, C.P., Vaziri, V., Aphale, S.S., 2023. Enhancing the drilling efficiency through the application of machine learning and optimization algorithm. Eng. Appl. Artif. Intell. 126, 107035.
Chen, X., Fan, H., Guo, B., Gao, D., Wei, H., Ye, Z., 2014. Real-time prediction and optimization of drilling performance based on a new mechanical specific energy model. Arabian J. Sci. Eng. 39 (11), 8221–8231.
Chen, X., Gao, D., Guo, B., Feng, Y., 2016. Real-time optimization of drilling parameters based on mechanical specific energy for rotating drilling with positive displacement motor in the hard formation. J. Nat. Gas Sci. Eng. 35, 686–694.
Chen, X., Du, X., Weng, C., Yang, J., Gao, D., Su, D., Wang, G., 2024. A real-time drilling parameters optimization method for offshore large-scale cluster extended reach drilling based on intelligent optimization algorithm and machine learning. Ocean Eng. 291, 116375.
Dashevskiy, D., Dahl, T., Brooks, A.G., Zurcher, D., Lofts, J.C., Dankers, S., 2008. Dynamic depth correction to reduce depth uncertainty and improve MWD/LWD log quality. SPE Drill. Complet. 23 (1), 13–22.
Ejike, C., Obuobi, I.F., Avinu, S., Abid, K., Teodoriu, C., 2024. Investigation and analysis of influential parameters in bottomhole stick–slip calculation during vertical drilling operations. Energies 17 (3), 622.
Elzenary, M.N., 2023. Real-time solution for down hole torque estimation and drilling optimization in high deviated wells using artificial intelligence. In: SPE/IADC Middle East Drilling Technology Conference and Exhibition.
Graves, A., Schmidhuber, J., 2005. Framewise phoneme classification with bidirectional LSTM and other neural network architectures. Neural Netw. 18 (5–6), 602–610.
Greff, K., Srivastava, R.K., Koutník, J., Steunebrink, B.R., Schmidhuber, J., 2016. LSTM: a search space odyssey. IEEE Transact. Neural Networks Learn. Syst. 28 (10), 2222–2232.
Hareland, G., Wu, A., Rashidi, B., 2010. A drilling rate model for roller cone bits and its application. In: SPE International Oil and Gas Conference and Exhibition in China.
Hegde, C., Wallace, S., Gray, K., 2015. Using trees, bagging, and random forests to predict rate of penetration during drilling. In: SPE Middle East Intelligent Oil and Gas Symposium.
Heydari, O., Sahraei, E., Skalle, P., 2017. Investigating the impact of drillpipe's rotation and eccentricity on cuttings transport phenomenon in various horizontal annuluses using computational fluid dynamics (CFD). J. Petrol. Sci. Eng. 156, 801–813.
Kang, W.C., McAuley, J., 2018. Self-attentive sequential recommendation. In: 2018 IEEE International Conference on Data Mining (ICDM). IEEE, pp. 197–206.
Khoshouei, M., Bagherpour, R., 2023. Measurement, prediction, and modeling of the drilling specific energy by soft rock properties during the drilling operation. Measurement 222, 113679.
Krizhevsky, A., Sutskever, I., Hinton, G.E., 2017. ImageNet classification with deep convolutional neural networks. Commun. ACM 60 (6), 84–90.
Li, G., Song, X., Zhu, Z., Tian, S., Sheng, M., 2023. Research progress and the prospect of intelligent drilling and completion technologies. Petrol. Drill. Techn. 51 (4), 35–47.
Li, Z., Song, X., Yu, Q., Gong, N., Jiang, Z., Zhu, Z., Zhang, C., 2025. Integrating mechanics and machine learning for build-up rate prediction. Geoenergy Sci. Eng. 246, 213594.
Liu, X., Bian, H., Wang, Y., Yang, Z., Luan, T., Kang, H., Hou, P., 2020. Characteristics and suggestions of global oil and gas exploration. Oil Forum 38 (6), 43.
Liu, J., Liu, J., Luo, X., 2021. Research progress in attention mechanism in deep learning. Chin. J. Eng. 43 (11), 1499–1511.
Marck, J., Detournay, E., Kuesters, A., Wingate, J., 2014. Analysis of spiraled-borehole data by use of a novel directional-drilling model. SPE Drill. Complet. 29 (3), 267–278.
Marquez, F.J., 2021. Drilling optimization applying machine learning regression algorithms. In: Offshore Technology Conference.
Maurício, J., Domingues, I., Bernardino, J., 2023. Comparing vision transformers and convolutional neural networks for image classification: a literature review. Appl. Sci. 13 (9), 5521.
Mazen, A.Z., Rahmanian, N., Mujtaba, I., Hassanpour, A., 2021. Prediction of penetration rate for PDC bits using indices of rock drillability, cuttings removal, and bit wear. SPE Drill. Complet. 36 (2), 320–337.
Motahhari, H.R., Hareland, G., James, J.A., 2010. Improved drilling efficiency technique using integrated PDM and PDC bit parameters. J. Can. Petrol. Technol. 49 (10), 45–52.
Negara, A., Saad, B., 2020. Combining insight from physics-based models into data-driven model for predicting drilling rate of penetration. In: International Petroleum Technology Conference. IPTC.
Oyedere, M., Gray, K., 2020. Torque-on-bit (TOB) prediction and optimization using machine learning algorithms. J. Nat. Gas Sci. Eng. 84, 103623.
Pan, S.Y., Liao, Q., Liang, Y.T., 2022. Multivariable sales prediction for filling stations via GA improved BiLSTM. Pet. Sci. 19 (5), 2483–2496.
Qi, P., Chen, Y., Temple, P., Li, W., Liu, L., Gao, F., Yang, J., Zhang, H., Lu, C., Tian, P., Liu, S., 2025. Coupled drilling optimization based on hybrid physics-machine learning models. In: Offshore Technology Conference. OTC. D041S054R007.
Quitian-Ardila, L.H., Garcia-Blanco, Y.J., Rivera, A.D.J., Schimicoscki, R.S., Nadeem, M., Calabokis, O.P., Ballesteros-Ballesteros, V., Franco, A., 2024. Developing a machine learning-based methodology for optimal hyperparameter determination—A mathematical modeling of high-pressure and high-temperature drilling fluid behavior. Chem. Eng. J. Adv. 20, 100663.
Reza, M.R., Alcocer, C.F., 1986. A unique computer simulation model well drilling: part II—The drilling model evaluation. In: SPE Western Regional Meeting. SPE. SPE-15109-MS.
Salminen, K., Cheatham, C., Smith, M., Valiullin, K., 2017. Stuck-pipe prediction by use of automated real-time modeling and data analysis. SPE Drill. Complet. 32 (3), 184–193.
Shaabani, E., Rezaeian, M., Moein, M.J.A., Maarefvand, P., 2016. Experimental investigation into rate of penetration in carbonated rocks. Int. J. Oil Gas Coal Technol. 11 (4), 339–349.
Sutskever, I., Vinyals, O., Le, Q.V., 2014. Sequence to sequence learning with neural networks. Adv. Neural Inf. Process. Syst. 27.
Urdaneta, C., Jeong, C., Wu, X., Chen, J., 2024. Deep learning method for improving rate of penetration prediction in drilling. SPE J. 29, 3440–3448.
Vaswani, A., Shazeer, N., Parmar, N., Uszkoreit, J., Jones, L., Gomez, A., Kaiser, L., Polosukhin, I., 2017. Attention is all you need. Adv. Neural Inf. Process. Syst. 30.
Wu, Z., Wang, Z., Gu, Y., Wang, S., Kou, T., 2024. Intelligent prediction model of downhole weight on bit based on GA-Bi-LSTM and its application. In: Proceedings of the 2024 2nd International Conference on Advances in Artificial Intelligence and Applications, pp. 210–217.
Yang, J., Li, L., Song, Y., Tong, G., Zhang, M., Zhang, H., 2023. Current status and prospects of offshore oil and gas drilling technology development in China. Acta Pet. Sin. 44 (12), 2308.
Yehia, T., Gasser, M., Ebaid, H., Meehan, N., Okoroafor, E.R., 2024. Comparative analysis of machine learning techniques for predicting drilling rate of penetration (ROP) in geothermal wells: a case study of FORGE site. Geothermics 121, 103028.
Zhao, J., Huang, W., Gao, D., 2022. Research on dynamic prediction of tubular extension limit and operation risk in extended-reach drilling. J. Nat. Gas Sci. Eng. 107, 104542.
Zhou, F.Y., Jin, L., Dong, J., 2017. Review of convolutional neural network. Chin. J. Comput. 40 (6), 1229–1251.